Journal of Applied Electrochemistry (2005) 35:101–111
DOI 10.1007/s10800-004-4062-1

Copper recovery in a spouted vessel electrolytic reactor (SBER)

P.A. SHIRVANIAN and J.M. CALO*
Brown University, Division of Engineering, Providence, RI 02912, USA
*(*author for correspondence, e-mail: Joseph_Calo@brown.edu)*

Received 1 November 2003; accepted in revised form 17 August 2004

Key words: copper backstripping, copper electrowinning, spouted bed particulate electrode

Abstract

An investigation of copper recovery from acidic solutions in a particulate, cylindrical spouted vessel of conductive particles is presented. The effects of current, initial copper ion concentration, supporting electrolyte concentration, particle loading, liquid flow rate, solution pH, and temperature on copper recovery rate, current efficiency and energy efficiency of the electrolytic deposition process were investigated under galvanostatic conditions. Experiments were also conducted to investigate the effects of backdissolution or 'backstripping' of the deposited metal in the acidic solution. It is hypothesized that the latter occurs *via* both chemical and electrochemical anodic oxidation in the bed of conductive particles. It was found that sparging of the electrolyte solution with selected gases to remove dissolved oxygen increased the current efficiency by as much as 30% under certain conditions. Finally, a numerical kinetic model of electrochemical deposition and backstripping, coupled with mass transfer in the particulate cathode bed, is presented that describes the behaviour of the net copper recovery curves reasonably well.

List of symbols

a	electrode area per unit volume (m^{-1})
C_j	concentration of species j (mol m^{-3})
C_{js}	concentration of species j at electrode surface (mol m^{-3})
C	metal cation concentration in solution, initial (ppm or mol m^{-3})
C_O	initial metal cation concentration in solution, initial (ppm or mol m^{-3})
d_p	particle diameter (m)
D	diffusion coefficient (m^2 s^{-1})
E_b	apparent activation energy (backstripping) (kJ mol^{-1})
E	electrode potential (V)
F	Faraday's constant (C mol^{-1})
i	total current density (A m^{-2})
i_j	current density of reaction step j (A m^{-2})
k_j	electrochemical rate constant (m s^{-1})
k_L	mass transfer coefficient (m s^{-1})
k_0	electrochemical rate parameter (m s^{-1})
$k_{0,b}$	backstripping rate constant pre-exponential factor (ppm min^{-1})/(mol $kg^{-1}bar^{-1}$)
K_B	backdissolution rate (mol m^{-3} s^{-1})
K_H	Henry's law constant for oxygen in water (mol oxygen (kg water)$^{-1}$ (bar^{-1})
n	apparent reaction order
n_j	number of electrons in rate j
r_b	backstripping rate (ppm min^{-1})
r_j	rate of reaction or mass transport (mol m^{-3} s^{-1})
R	gas constant (J K^{-1} mol^{-1})
Re_p	particle Reynolds number ($= u\, d_p/v$)
Sc	Schmidt number ($= v/D$)
Sh	particle Sherwood number ($= k_L d_p/D$)
t	time (s)
T	temperature (K)
ΔH_0^*	heat of activation at equilibrium potential (kJ mol^{-1})
α	transfer coefficient (Equation 10)
v	kinematic viscosity (m^2 s^{-1})

1. Introduction

Electrolytic recovery of metals from aqueous solutions is important in a number of applications, including the production of metals, metal plating, and their removal from wastewaters. Packed particulate and porous electrodes have been shown to be effective for electrolytic removal of metal ions from aqueous solutions. However, these types of electrodes are ultimately limited by particle agglomeration and/or plugging of the porosity (e.g., [1]). Fluidized bed electrodes circumvent some of these problems (e.g., [2]); however, their current-carrying capacity is limited. In addition, measurements of potential distributions in fluidized beds have revealed the existence of anodic or pseudo-anodic zones that are not always

present in corresponding fixed beds [3]. The existence of anodic or bipolar regions was also observed by Hadzismajlovic [4], and was cited as one of the drawbacks of fluidized bed electrodes. Bisang [5] also predicted the formation of anodic zones in packed bed electrodes, which become more important with increasing bed depth.

Here we present an investigation of the behaviour of a cylindrical spouted bed of conductive particles as a cathode for electrolytic recovery. Spouted bed electrodes are, in a sense, a hybrid of fixed (packed) and fluidized bed electrodes, incorporating advantages of both, while minimizing some of their disadvantages. There are relatively few studies in the literature on similar devices. Copper electrowinning from acidic solutions was examined in small, related devices by Jiricny et al. [6], Stankovic and Stankovic [7], Masterson and Evans [8], and Scott [9]. Also, Evans and coworkers reported on zinc electrowinning in a spouted bed electrode [10]. In the work of Stankovic [7] and Evans and coworkers [8], the cathode particles were fluidized and the cathode and anode compartments were separated. This minimized the reaction of dissolved oxygen produced at the anode with deposited metal, resulting in high current efficiencies [8]. However, in this arrangement electrical contact between particles in the vicinity of the cathode and between particles is provided via random chains of particles that form only momentarily, which can limit the recovery rate [11].

2. Experimental details

2.1. *Cylindrical spouted bed apparatus*

A conceptual schematic of the spouted bed apparatus and flow system is presented in Figure 1. As shown, the liquid is introduced as a high velocity jet at the center of the bottom of the conical vessel. This liquid jet, known as the 'spout', entrains particles fed from the bottom cathodic cone. After passing through the draft tube, the entrained particles disengage from the liquid flow in a region known as the 'fountain', and then fall on top of the inverted conical distributor. The collector/distributor cone channels the particles to the periphery of the reactor, where they fall onto the particulate cathode that moves them inward and downward back to the entrainment region. The pumping action provided by the spout circulates the particles through the vessel in a toroidal fashion; upwards in the spout, and downwards in the annular moving bed. Liquid also flows outward and upward through the annular downward moving bed of particles.

A diagram of the SBER is presented in Figure 2. The reactor body was made from 12 inch (0.305 m) plexiglass tubing. The conical bottom section was made from 1/16 inch (0.16 cm) plexiglass sheet. A 2.54 cm diameter draft tube was used to contain and stabilize the spout. Three, 316 stainless steel studs, located 120° apart, were used to provide the cathodic connection to the conductive bed particles on the conical vessel bottom. The anode was constructed from expanded platinized niobium mesh on a plastic support, which was used to position and hold the anode in place below the collector/distributor, parallel to the cathode. The areas of the cathode and anode were 0.0823 m^2 and 0.0334 m^2, respectively. The separation distance between the electrodes was set at a constant value of 3.81 cm for all the experiments, which was much greater than necessary to accommodate a wide range of particle loading in order to explore the effects of this parameter on SBER performance. For particular applications, however, it is expected that this distance would be significantly reduced and optimized. The anode and frame were enclosed in a fine polypropylene mesh to prevent electrical contact with the particles. A plastic deflector for the bed media disengaging from the spout was incorporated in the form of a disc fixed directly above and normal to the spout flow. A variable 50 A d.c. power supply was used to deliver current to the SBER. The electrolyte solution was circulated using a magnetically coupled centrifugal pump equipped with a bypass valve for flow rate control. A paddle wheel flow meter (Signet 3-2535) was used to measure the liquid flow rate.

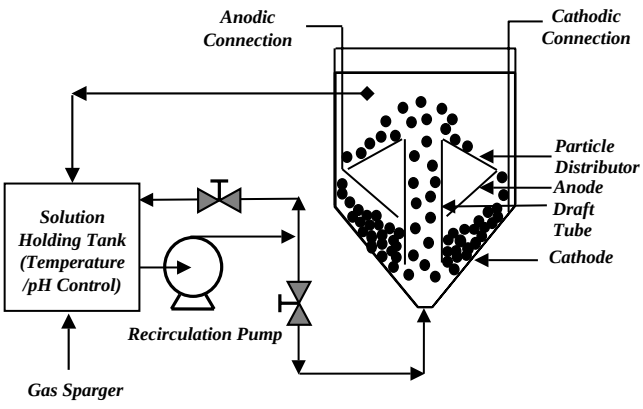

Fig. 1. Schematic of SBER apparatus and flow system.

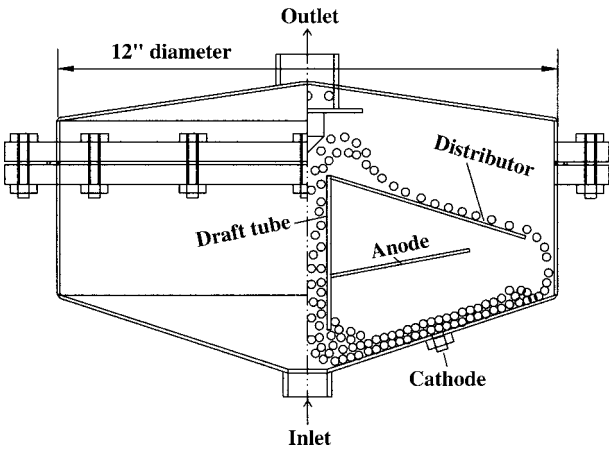

Fig. 2. Schematic of 12 inch Spouted bed electrolytic reactor (SBER).

The granular media were 2 mm diameter glass spheres, metallized with a layer of electroless nickel, followed by an electroplated layer of copper. The standard copper sulfate solution used for all the electrowinning experiments consisted of 70 g $CuSO_4.5H_2O$, (>98%, Aldrich) added to distilled and deionized water to a total volume of 18 l. 130 g of Na_2SO_4 (granular, >99%, Aldrich) were added to this solution, as well as sufficient sulfuric acid (1 M, Mallinkrodt) and potassium hydroxide (1 M, Fisher Scientific) to attain the desired pH. An automatic pH controller (Barnant, model HD-PHP) was used to maintain constant pH with KOH solution. Similarly, during metal backdissolution experiments, sulfuric acid solution was used for pH control using the same controller.

2.2. *Experimental procedures*

Metal ion concentrations in solution were measured by atomic absorption spectroscopy (AAS; Buck Scientific, model 210 VGP), and the total amount of metal recovered was determined by difference. An atomic absorption standard calibration solution of 996 μg ml^{-1} copper in 2% HNO_3 and a blank solution were used to calibrate the AAS. Samples were diluted to 1/100 of the original concentration to perform AAS analysis. The instrument manual for the copper lamp lists the following specifications: wavelength 324.8 nm, slit 0.7 nm, detection limit 0.02 mg l^{-1}, linear range 3 mg l^{-1} and flame type AA, lean/blue.

Superficial current densities were determined by dividing the total steady-state current by the cross sectional area of the bed. The amount of metal, which would be recovered at 100% efficiency, was calculated by multiplying the ampere-hours of delivered current by the electrochemical gram equivalent of the particular metal (i.e., Faraday's law). The actual amount of recovered metal was then divided by this value to yield the current efficiency.

In selected cases, backdissolution or backstripping experiments were conducted by first operating in the normal metal recovery mode, and then turning off the current while maintaining constant flow and particle recirculation rate, and monitoring the dissolved metal concentration as a function of time. Backstripping tests performed using the same procedure while sparging with oxygen yielded similar results, so it was concluded that the dissolved oxygen concentration remained relatively constant over the time-scale of these experiments.

The effects of solution temperature on copper recovery were investigated by thermostatting the electrolyte solution holding tank. Since the solution tended to heat up gradually over the course of an experiment, this was accomplished by immersing a coil of stainless steel tubing in the solution reservoir through which cold water flowed continuously. A resistive heater immersed in the solution was used to set the desired solution temperature to within ± 1 °C over the course of a typical experiment. The 'standard case' parameter set selected was: T=35 °C; pH 2.5; I=10 A; 130 g sodium sulfate, 70 g copper sulfate in 18 l of water; volumetric flow rate of 27.2 l min^{-1}; and 600 cm^3 of conductive bed media.

3. Results

The principal reactions that occur during copper electrowinning from acidic aqueous solutions are [10, 12]:
Main cathodic reaction:

$$Cu^{2+} + 2e^- = Cu \quad (1)$$

Side reaction at the cathode:

$$2H^+ + 2e^- = H_2 \quad (2)$$

Main anodic reaction:

$$2H_2O = 4H^+ + 4e^- + O_2 \quad (3)$$

Thus, oxygen is generated at the anode, and hydrogen can be generated as a byproduct at the cathode. In acidic solutions, dissolved oxygen can also spontaneously oxidize deposited metal on the particle via:

$$Cu + \frac{1}{2}O_2 + 2H^+ = Cu^{2+} + H_2O \quad (4)$$

3.1. *Effects of temperature, pH, and oxygen on copper recovery in the SBER*

The effect of temperature on copper recovery is presented in Figure 3 at a constant pH of 2.5. The copper ion concentrations in this figure were normalized by the initial value in each case (about 1000 ppm). The linear reference curve represents the ideal recovery process

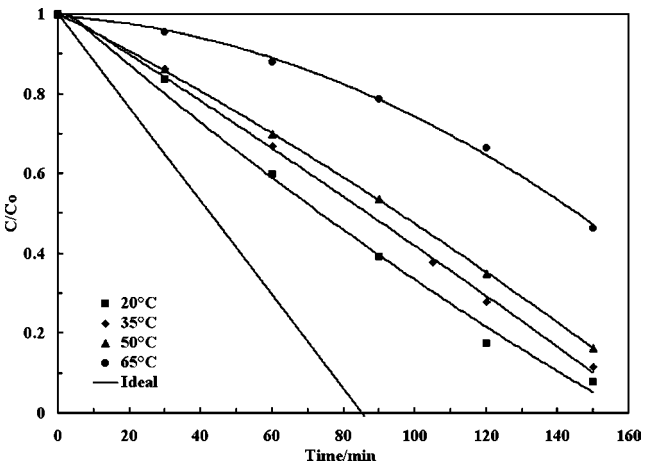

Fig. 3. Net copper recovery at pH 2.5 as a function of solution temperature.

according to Faraday's law at 100% current efficiency in the absence of mass transfer limitations and any other effects. The data in Figure 3 are presented in terms of current efficiency (i.e., the derivative of the recovery curve) in Figure 4. As shown in this figure, the current efficiencies at a pH of 2.5 varied over the range of 0.46–0.59, 0.38–0.5, 0.4–0.48 and 0.12–0.29, at solution temperatures of 20, 35, 50 and 65 °C, respectively. At the two lowest pH values investigated of 2 and 2.5, it was found that increasing the solution temperature generally decreased the recovery rate. This trend became less pronounced with increasing pH, such that by a pH of 3 the current efficiencies at the four different temperatures were all similar.

In general, it was observed that the current efficiencies were slightly lower at the beginning of each run (cf. Figure 4). This behaviour is attributed primarily to higher electrical resistance due to an oxide layer that is initially present on the particle surfaces. This assumption is supported by slightly elevated voltages and current oscillations that are typically observed during the early stages of an electrodeposition experiment. The conductivity of the particles increases as metal begins to deposit. In most cases, the current efficiency remains relatively constant until near the end of the run where it decreases slightly, most probably due to increasing mass transfer limitations. Also, at 20 °C the current efficiency decreases as the pH increases from 2.5 to 3. This result is consistent with the data of Scott [9], wherein copper recovery was observed to be more efficient at low pH, due to the higher conductivity of the electrolyte. However, upon further decrease in pH from 2.5 to 2, the current efficiency decreases. Therefore, the optimum operating pH for 20 °C seems to be in the vicinity of 2.5. On the other hand, at 35 °C the current efficiency increases monotonically with decreasing pH from 3 to 2. At 50 °C and higher, however, the current efficiency decreases monotonically with decreasing pH. This behaviour is attributed to backdissolution or backstripping of deposited copper metal from the particles as a result of chemical and/or electrochemical oxidation.

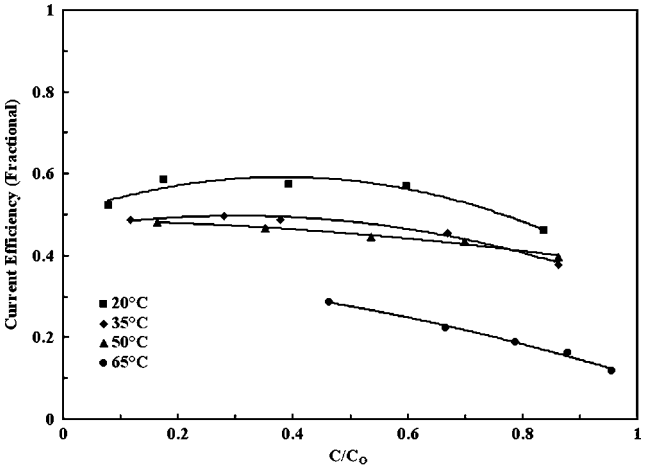

Fig. 4. Cumulative current efficiency at pH 2.5 as a function of temperature.

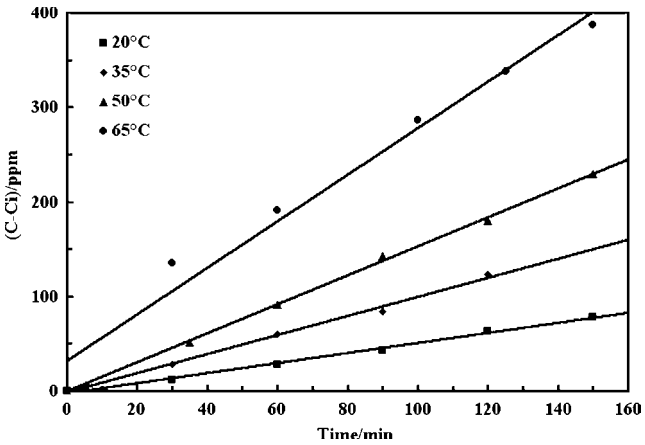

Fig. 5. Copper backdissolution via chemical oxidation as a function of temperature for pH 2.5.

According to Reaction 4, dissolved oxygen, produced by dissociation of water at the anode, in the presence of H^+ can re-oxidize the deposited metal to copper ions in solution. In order to investigate the role of this reaction in the SBER, backstripping experiments were conducted as described in the Experimental section. Copper backstripping data as a function of solution temperature are presented in Figure 5 at a pH of 2.5. As indicated, the rate of copper oxidation under these conditions exhibits close to zeroth order behaviour in copper ion concentration, and generally increases monotonically with temperature. The measured backstripping rates were: pH 2.5: 0.5, 0.9, 1.7 and 2.8 ppm min^{-1}; pH 2: 0.8, 1.2, 1.9, and 2.0 ppm min^{-1}; and pH 3: 1.1, 1.1, 1.5 and 2.1 ppm min^{-1}; all for temperatures of 20, 35, 50 and 65 °C, respectively. An Arrhenius plot of the backstripping rates is presented in Figure 6. From this Figure it is noted that the absolute rates do not vary very much with pH (except for the values at 20 °C, for which there is some scatter). If it is assumed that the reaction is zeroth order in pH, then the backstripping rate, r_b, behaves according to the following:

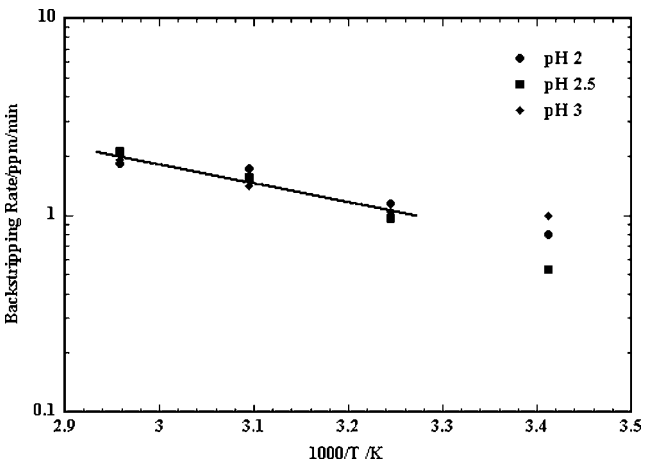

Fig. 6. Arrhenius plot of backstripping rates from Figure 5.

$$\ln(r_b) = \ln(k_{0,b}) - E_b/RT + n\ln([O_2]) \quad (5)$$

Assuming that the solution is saturated with oxygen at atmospheric pressure following the extended deposition run prior to each backstripping experiment, the Henry's law constant, K_H, can be used to estimate the dissolved oxygen concentration [13]:

$$\ln(K_H) = 1500/T(K) - 11.676 \quad (6)$$

A multiparameter fit of the data in Figure 6 yields an apparent reaction order close to unity with respect to oxygen, with $k_{0,b}=1.2 \times 10^8$ (ppm min^{-1}) (mol oxygen)$^{-1}$ (kg water) $\pm$ 2.1%, and $E_b=30 \pm 1$ kJ mol^{-1}. Although additional work would have to be done to elucidate the actual heterogeneous oxidation mechanism, these limited data suggest that the rate-limiting step involves the reaction of oxygen with metallic copper or an intermediate surface complex. The reaction step with $[H^+]$ would have to be rapid in order to account for the close to zeroth order behaviour with respect to hydrogen ion concentration. The relatively low apparent activation energy suggests the influence of mass transfer limitations, most probably with respect to oxygen transport to the particle surface.

The data of Ives and Rawson [14] show that the corrosion/dissolution of copper into acidic solution takes place at a constant rate for extended periods of time, consistent with the present results. These authors hypothesized that when immersed in an oxygenated aqueous medium, copper almost instantaneously forms a very thin film of oxide that is adherent and self-healing. This film does not grow beyond about 20 Å in thickness before mechanical strain forces its breakup, resulting in a porous oxide film. It was assumed that oxide film growth is based primarily on dissociative adsorption of dissolved oxygen and outward transport of copper ions. Furthermore, it was shown that the film thickness, while contributing to an increase in electrical resistance, never grows to a significant extent since any oxide that became insulated from the metal would either fall off or rapidly dissolve. In the moving bed cathode, the mechanical action between particles limits the formation and extent of oxide film. On the one hand, this maintains particle conductivity by removing oxide, but on the other hand it could enhance copper backdissolution via increasing the rate of oxide generation/removal. To explore this possibility, experiments were conducted for the 'standard case' parameter values, but at flow rates below the minimum spouting velocity where the particles tended to form a fixed bed on the conical bottom of the SBER. The results showed a decrease in the backdissolution rate to about 0.2 ppm min^{-1} (similar to the results in [14]) in comparison to $\sim$1 ppm min^{-1} while the reactor was spouting. Thus, mechanical action in the moving bed cathode may contribute to the measured net backdissolution rates.

Copper backdissolution may also be enhanced in anodic zones during electrodeposition in the particulate moving bed. The half-cell oxidation of copper (the reverse of Reaction 1):

$$Cu^0 = Cu^{2+} + 2e^-; \quad E^\circ = -0.337\,V$$

is the most favoured anodic reaction on the particles. Consumption of the electrons produced in this reaction will occur in the predominant surrounding, contiguous, cathodic zones by either the reverse reaction, which does not result in net copper backdissolution, or via the spontaneous half-cell reaction (reverse of Reaction 3):

$$2H^+ + 2e^- + \frac{1}{2}O_2 = 2H_2O; \quad E^\circ = +1.23V.$$

The sum of these two reactions results in the same overall exothermic backstripping reaction as Reaction 4. Thus, the existence of anodic zones in the particulate cathode can electrolytically enhance copper backstripping. Unfortunately, however, the relative or absolute magnitude of the anodic dissolution rate cannot be ascertained experimentally by simply shutting off the current.

To further explore the role of oxygen in the backstripping reaction, experiments were performed by sparging the electrolyte solution in the holding tank with air or argon. The effects of some of these experiments on net copper recovery are summarized in Figure 7 for a pH of 2.5 at 35 °C. Under these conditions, the current efficiency varied from 0.55 to 0.64 and the backstripping rate was 0.8 ppm min^{-1}, and from 0.48 to 0.68 with a backstripping rate of 0.4 ppm min^{-1}, for sparging with air and argon, respectively. The corresponding values at a pH of 2 were: 0.3–0.49 and 1.2 ppm min^{-1}; and 0.43–0.57 and 0.4 ppm min^{-1}, for sparging with air and argon, respectively. At a pH of 3, the resultant values were: 0.45–0.49 and 0.8 ppm min^{-1}; and 0.35–0.58 and 0.4 ppm min^{-1}, for sparging with air and argon,

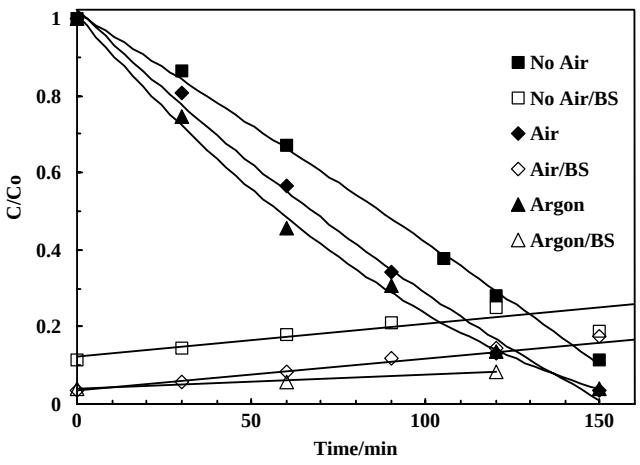

Fig. 7. Effects on copper recovery and corresponding backstripping of sparging electrolyte solution with air and argon at 35 °C at pH 2.5.

respectively. Thus, the recovery rate *increases* with gas sparging and appears to be similar for the two gases, especially at the higher pH values; and this effect diminishes with decreasing pH. This behaviour is consistent with the reduction of the dissolved oxygen concentration upon gas sparging.

3.2. *Electrodeposition model*

A numerical model was formulated to simulate the behaviour of the net copper recovery curves with pH and temperature. This was based on modifications of a general approach for modelling the behaviour of recirculating electrochemical reactors [15–17].

Assumptions

(i) At the cathodic electrode surface, an electrochemical reaction occurs of the type:

$$A^{n_1^+} + n_1 e^- \rightarrow M \tag{7}$$

(ii) Pseudo-steady-state behaviour in the mass transfer boundary layer at the electrode surface

(iii) Electrochemical kinetics are described by the Butler–Volmer, or in the limiting case, the Tafel equations (e.g., [18])

(iv) Electrochemical reaction is first order, and the backstripping reaction is zeroth order in copper ion concentration

(v) Transport of ionic reactants by migration is negligible due to the excess of supporting electrolyte.

The rate of mass transfer of species, j, with bulk concentration of C_j, is given by

$$r_j = k_L(C_j - C_{js}) \tag{8}$$

The rate of electrochemical reaction is given by

$$r_j = k_j C_{js} = \frac{i_j}{n_j F} \tag{9}$$

where k_j is an electrochemical rate constant, which is dependent upon the electrode potential, E, according to the Tafel approximation:

$$k_j = k_{j0} \exp\left(\frac{\alpha n F E}{RT}\right) \tag{10}$$

The total rate is equal to the current density divided by the number of Faradays of charge required to convert one mole of species (i.e., i_j/n_jF). At steady-state, the rates in Equations 8 and 9 are equal, resulting in the expression for the surface concentration of species j:

$$C_{js} = \frac{C_j}{1 + k_j/k_L} \tag{11}$$

which can then be eliminated from Equation 9, resulting in

$$r_j = k_j \frac{C_j}{1 + k_j/k_L} \tag{12}$$

in which the ratio, k_j/k_L, determines the degree of mass transfer limitation.

For galvanostatic operation, the total current from Reactions 1 and 2 is given by

$$i = i_1 + i_2 = \frac{n_1 F k_1 C_1}{1 + k_1/k_L} + n_2 F k_2 \tag{13}$$

and the mass balance for metal cations becomes

$$\frac{dC_1}{dt} = -\frac{a i_1}{n_1 F} + K_B \tag{14}$$

where K_B is the total backdissolution rate due to all mechanisms, which is assumed to be zeroth order in metal cation concentration at constant oxygen concentration and pH.

The conditional exchange current density and transfer number, as defined in Tamamushi [19], for copper electrodeposition were taken as 0.04 A cm^{-2} and 0.5 [20], respectively. The exchange current density and transfer number for hydrogen evolution were taken to be 2×10^{-7} A cm^{-2} and 0.49 for copper electrodes [21]. The mass transfer coefficient was estimated from Pickett [22] for a single layer packed bed electrode:

$$Sh = 0.83(Re_P)^{0.56} Sc^{1/3} \tag{15}$$

The variation of exchange current density, i_0, is given by

$$\frac{d(\ln i_0)}{dT} = \frac{-\Delta H_0^*}{RT^2} \tag{16}$$

where ΔH_0^* is the heat of activation at the equilibrium potential [20]. The values used for copper and hydrogen are 167.0 kJ mol^{-1} at 25 °C [20] and 46.4 kJ mol^{-1} at 20 °C [21], respectively.

Solution methodology:

(i) With fixed current density and initial concentration of copper ions, C_{10}, the current balance given by Equation 13 is solved numerically using the method of bisection (e.g., [23]) to give the initial electrode potential, E_0.

(ii) Equation 14 is solved by marching in time, using a Runge–Kutta, 4th order method [24].

(iii) Steps (i) and (ii) are repeated until the desired time is reached.

The results of numerical simulations of the 'standard case' (Section 2) are presented in Figure 8 with current as a parameter. As shown, the simulation explains the experimental data reasonably well. Initially, the deposition process is kinetically limited, and after passing through a regime of 'mixed' control, becomes fully mass transfer limited.

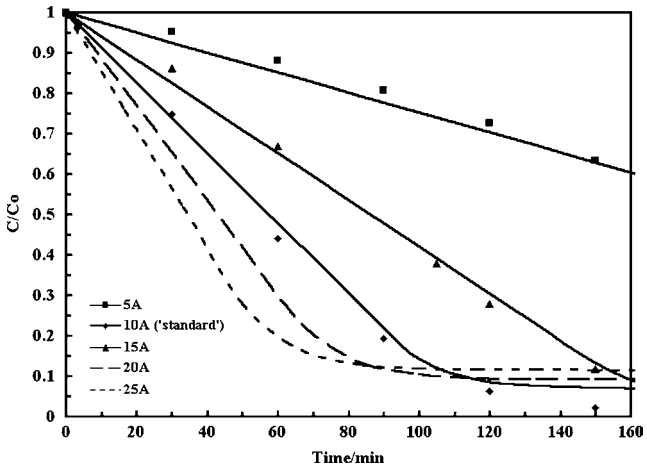

Fig. 8. Model results and experimental data for pH 2.5 at 35 °C as a function of current. Results for currents 20 and 25 A are from the simulation only.

The backstripping rates used in the simulations were initially assumed to be those measured in the backstripping experiments with the current shut off. However, in general it was found that *greater* backstripping rates were required to match the experimental results, which increased with current. For currents of 5, 10, 15, 20 and 25 A, the requisite backstripping rates required to match the data in Figure 8 were 2.5, 4, 6, 8 and 10 ppm min^{-1}, respectively, in comparison to the experimental values obtained by simply shutting off the current that were on the order of 1 ppm min^{-1}. The larger values, plus the dependence on current is consistent with enhanced backstripping due to the existence of anodic zones (e.g., [25]).

In Figure 9, simulation results are compared with experimental data for the 'standard case' (10 A) with temperature as a parameter. The backstripping rates used in these simulations were 3.6, 4.0, 4.8 and 5.9 ppm min^{-1} for temperatures of 20, 35, 50 and 65 °C, respectively. It is noted that at the higher temperatures of 50 and 65 °C, SBER operation remains in the 'mixed' zone of combined reaction/mass transfer-rate control for a greater portion of the concentration history, in comparison to that at the lower temperatures of 20 and 35 °C. This is consistent with greater mass transfer resistance as the kinetic rate constants increase more rapidly with temperature.

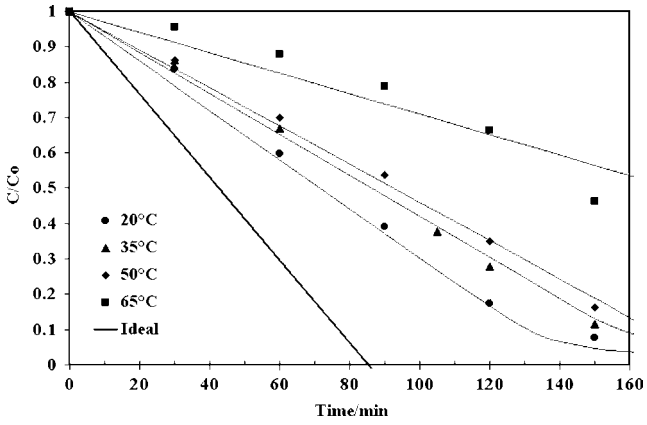

Fig. 9. Model results and experimental data at a current of 10 A, for pH 2.5 as a function of solution temperature.

3.3. *Parametric studies*

Parametric studies were performed to investigate the sensitivity of copper recovery in the SBER to a few key variables by defining a 'standard case' parameter set (Section 2), and varying one parameter at a time, while holding all the others constant.

As shown in Figure 10, increasing the current (density) from 5 to 15 A has a positive effect on recovery rate, and hence current efficiency, as expected.

As shown in Figure 11, increasing the volumetric flow rate from 23.5 to 27.2 ('standard case') l min^{-1}, initially decreases the recovery rate, and it then remains essentially constant up to 37.8 l min^{-1}. (At the highest flow rate, the recovery rate increases slightly at low concentrations.) From these results, it can be concluded that the best operating flow rate is the lowest that can still keep the bed spouting, while exceeding the inception

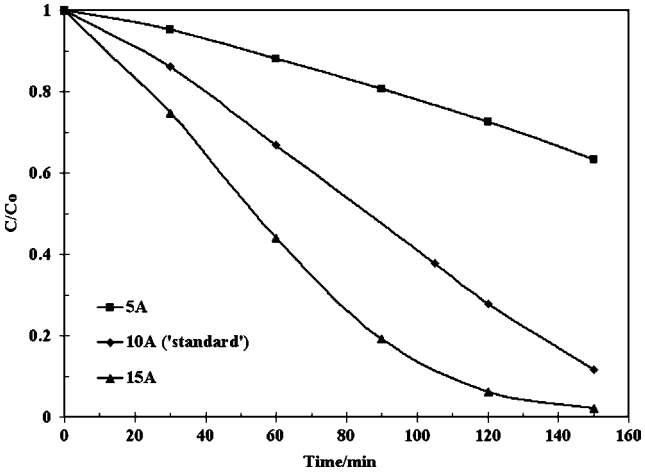

Fig. 10. Effect of current on copper recovery rate.

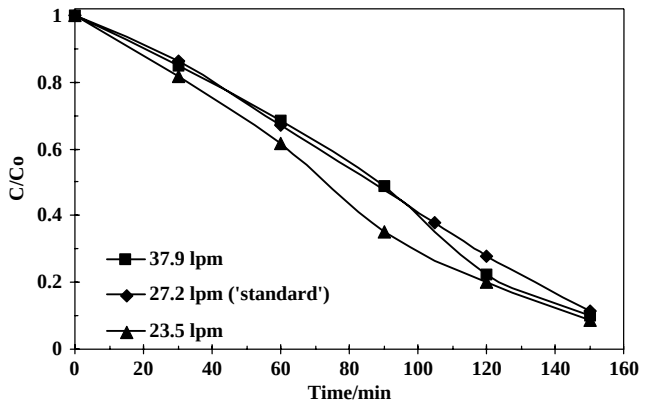

Fig. 11. Effect of volumetric flow rate on copper recovery rate.

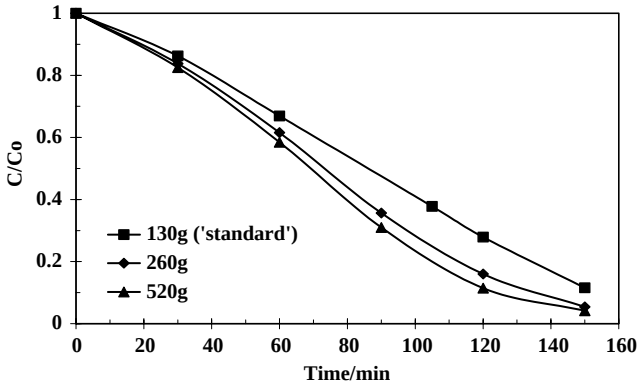

Fig. 12. Effect of supporting electrolyte concentration (g Na_2SO_4 per 18 l) on copper recovery rate.

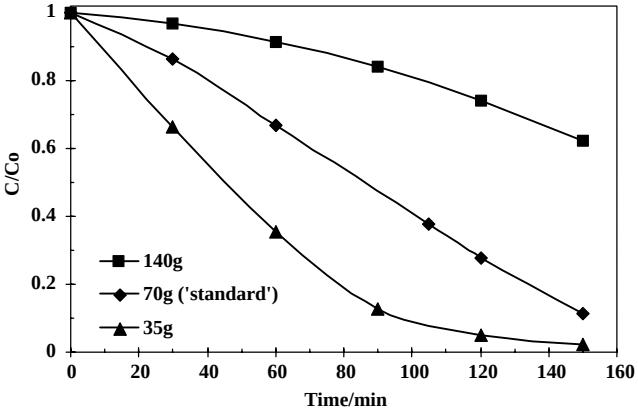

Fig. 13. Effect of copper sulfate concentration (g $CuSO_4$ per 18 l) on copper recovery rate.

point for particle agglomeration in the moving bed cathode.

From the results in Figure 12, it is apparent that the recovery rate and current efficiency increase with concentration of supporting electrolyte. However, both approach asymptotic limits at the highest concentrations. Addition of supporting electrolyte generally increases solution conductivity and electrodeposition. It also decreases the required voltage. For example, the voltage required to pass 10 A decreased from 7.8 to 4.5 V as the supporting electrolyte concentration was quadrupled. This is consistent with Gouy–Chapman theory [26] which shows that the surface potential of the electrode decreases upon addition of supporting electrolyte for constant surface charge density. This reduces the effective potential experienced by copper ions near the electrode, thereby reducing the reaction rate, as approximated by the Tafel equation (Equation 10). Therefore, at some point the reduction in potential, and hence the electrodeposition reaction rate, offsets the gain due to increased conductivity of the solution due to additional supporting electrolyte, thereby rendering the additional electrolyte less effective.

As shown in Figure 13, the voltage required for passing the 'standard current' of 10 A decreases as the concentration of copper sulfate increases, due to increased conductivity of the electrolyte solution (similar to the effect of the supporting electrolyte).

The results in Figure 14 show that decreasing the particle loading increases the recovery rate, and thus the current efficiency, by as much as 30%. This increase in performance persisted down to 50% of the 'standard loading'. Further decreases in loading, however, resulted in instances of particle agglomeration. This was quite evident at 1/6 of the 'standard' loading, which corresponds to approximately a sparse monolayer of particles on the cathode. Under these conditions, the particulate bed tended to 'freeze'. Operation was continued by manually vibrating the bed every few minutes to disengage the particles from each other in order to keep the cathode bed moving and the vessel spouting. To explore the nature of the observed agglomeration at the

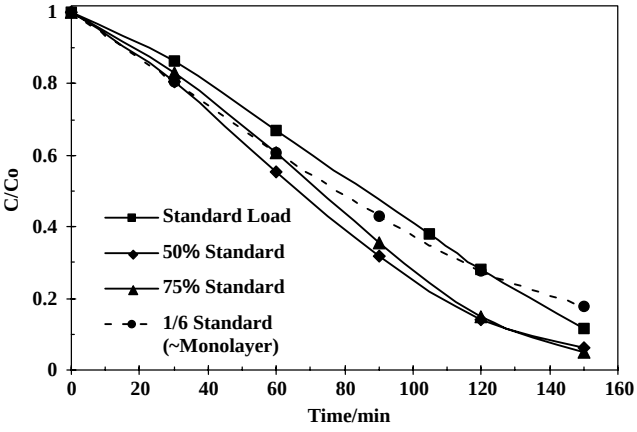

Fig. 14. Effect of particle loading on copper recovery rate ('standard load = 600 cm^3).

lowest loading, the conditions were replicated without copper sulfate in solution. No agglomeration was observed under these conditions. Thus, it was concluded that the observed agglomeration was due to the binding together of particles by fine 'fillets' of deposited metal at the high deposition rates induced, and not just coulombic forces due to particle polarization in the electric field.

The data showed that pH control did not have much of an effect. With no control, the pH tended to increase steadily during a typical three-hour experimental run (e.g., from 2.0 to 2.5). This conclusion is supported by the resultant current efficiency results that show just a 10% difference for pH values of 2 and 2.5 at 35 °C. This difference, however, increases rapidly at higher temperatures, where backstripping becomes more important.

4. Discussion

Much of the preceding results can be interpreted in terms of the reactive behaviour of the particles in the moving bed cathode. Using a fluidized/fixed bed electrode system, Hutin and Coeuret [27] found that a thin

bed behaved cathodically at every point, but that electrochemical activity increased rapidly with distance from the current feeder. For deeper beds, positive values of the overpotential, characterizing anodic behaviour, appeared in the distribution. It was concluded that the extent and influence of anodic zones increases with increasing bed expansion (i.e., bed void fraction) and bed height. Bisang [5] also showed that in a fixed bed, current efficiency decreases with distance into the bed. Bareau and Coeuret [28] investigated the anodic dissolution of copper in a fluidized bed electrode by measuring the overpotential distribution along the bed height. Similarly, Germain and Goodridge [2] discussed this problem and suggested that the optimum conditions for limiting anodic backdissolution would be to operate at low bed expansion and high current densities; conditions which also favour particle agglomeration, as verified by the present results with the 1/6 'standard load' (cf. Figure 14).

Storck and coworkers [29, 30] presented a detailed analysis and experimental results for a perpendicular design (i.e., electrolyte flow perpendicular to current flow), that showed large overpotentials near the current feeder (cathode). Kusakabe and Morooka [31] measured the overpotential in a fluidized bed electrode during copper electrodeposition and concluded that the most active regions in the bed were near the current feeder and near the membrane furthest away from the feeder. Our CFD simulation results [32] show that the flow of electrolyte through the moving bed on the cathode has significant components both parallel and perpendicular to the electric field. Therefore, it is expected that the most active particles will be located either near the current feeder or at the top of the moving bed. The particles in between these two regions are expected to be less active in electrodeposition, and could be chemically oxidized by dissolved oxygen and/or electrochemically in anodic zones.

Goodridge [33], Germain and Goodridge [2] and Hadzismajlovic [4] noted that electrode particles can be monopolar or bipolar. As experimentally observed, and validated in our CFD simulations [32], at any time, the bulk of the particle inventory resides on the cathode, forming a slowly moving bed. It is expected that these particles are predominantly monopolar, but there may also be a small fraction that is bipolar; for example, particles entering and exiting the electric field from the distributor and at the entrainment point, respectively, or that momentarily disengage from the moving bed due to hydrodynamics or particle mechanical action.

Saleh and Weidner [34] experimentally determined the current distribution in a packed bed operating in the parallel flow mode (i.e., electrolyte flowing parallel to current), and concluded that only the top fraction of the fixed bed nearest the anode effectively participates in electrodeposition, and that this fraction decreases with increasing electrolyte flow rate. This is supported by the work of Hutin and Coeuret [27] and Doherty et al. [35] who noted that the penetration depth of the current is limited by ohmic loss in the electrolyte. It was concluded that in order to achieve a maximum deposition rate per unit volume, the electrode should be no deeper than the penetration depth. Under the present 'standard case' conditions in the SBER, the moving bed can be as much as eight particles deep. In addition, the moving bed cathode exhibits a mean bed void fraction greater than that in a conventional fixed bed [32]. These factors both favour the formation of anodic zones [28]. Also, inactive particles provide additional surface area for spontaneous chemical oxidation via reaction (4) (e.g., [8]). Thus, the optimum moving bed depth is a function of a number of factors.

In addition to particle loading, current density, is a critical operating parameter in particulate electrode systems. As already indicated, anodic zones can form in the moving bed cathode if the current density is not sufficiently high. Sabacky and Evans [36] were among the first to introduce the concept of an effectiveness factor in a fluidized bed electrode as the ratio of total deposition rate to the rate when bed and electrolyte exhibit zero resistance. Similarly, Scott [37] defined an effectiveness factor in a particulate bed as the fraction of electrode area that effectively contributes to electrodeposition. This factor can be used to 'correct' the maximum attainable reaction rate, based on a uniform potential distribution in a packed bed electrode, to predict the actual rate. It was shown that the effectiveness factor initially decreases with increasing current density, but then at some point begins to increase with increasing current density. The decrease in effectiveness was shown to be a strong function of the limiting current density and hence the mass transport rate. As mass transport resistance increases, the current density required to maintain the effectiveness increases exponentially; and thus this will ultimately not be the most feasible approach to increasing effectiveness.

At high cathodic overpotentials, where the SBER is typically operated, the primary mass transport mechanism of metal ions to the surface of the cathode particles is ordinary Fickian diffusion. At very low current densities, the concentration of metal ions at the particle surface is essentially the same as in the bulk electrolyte solution, and the rate of reduction at the cathode will be proportional to the current density. At higher current densities, however, the ion concentration becomes depleted at the surface, and the rate of metal reduction becomes limited by the diffusion rate of metal ions to the cathode surface. Under these conditions, the Nernst approximation of a linear concentration gradient in the diffusion layer yields a diffusion-limited current density of $i_L = -[Dn_jFC]/\delta$, where δ is the Nernst layer thickness which controls the limiting current density. This is the primary impetus for using porous or particulate electrodes with high interstitial liquid flow rates. As an example, the limiting current density for recovery of silver from a 1000 ppm silver cyanide solution with moderate agitation is approximately 0.6 A cm^{-2}. The current efficiency, however, typically begins to fall off at

current densities that are approximately an order of magnitude less than this, because as the metal ion concentration at the cathode decreases, other electrode reactions become appreciable. Therefore, to maintain high current efficiency, the system should be operated at lower current densities. Consequently, the optimum current density must be defined with respect to the overall process objective of maximizing recovery rate or cost.

The dependence of the recovery performance of the SBER on volumetric flow rate is complex. Increasing the inlet jet flow rate produces a higher flow rate through the moving bed, which tends to decrease δ and enhance the mass transfer rate. However, this is roughly dependent on the superficial velocity to the 0.5–0.6 power, which can be easily offset or nullified by a number of other factors. For example, we have shown that increasing the inlet velocity can *decrease* the particle circulation rate [32, 38]. This is because the increased flow up through the moving bed presents a greater resistance to the movement of particles down to the entrainment region. This behaviour slows the mean particle velocity in the moving bed and thus increases the particle residence time in the cathode, which under certain conditions could actually improve recovery performance. However, it also increases the mean bed depth that results in an increased fraction of inactive particles and greater backdissolution of deposited metal. It is this latter behaviour that is believed to be controlling much of the recovery data presented in Figure 11. It is noted, however, that the recovery performance at the highest flow rate improves significantly as the copper ion concentration becomes very low. This latter behaviour is consistent with the improved mass transfer rate due to the higher flow rate manifesting itself under the mass transfer-controlled conditions at low concentrations.

5. Conclusions

The SBER system investigated in this work exhibited good performance for the recovery of copper from dilute solutions. It is shown that in general it is best to operate the system at low pH and low temperature. Higher pH results in higher overall resistance, and high temperatures generally increase the backdissolution rate. (However, similar conclusions may not apply for the recovery of other metals.)

It is shown that for optimum performance of the SBER, the cross section should be as large as possible to provide a high surface area for metal recovery. In addition, a slowly moving bed of active particles, on the order of just a couple of layers or so on the cathode is desirable from the point of view of optimizing the exposure of the electrolyte to particles in electrical contact with the current feeder, as well as in minimizing backdissolution effects. (Gas sparging may be employed to minimize dissolved oxygen levels in the case of a single electrolyte system, as reported here.) The particulate cathode bed must be kept moving in order to avoid particle agglomeration. The system should be designed such that optimum loading occurs near the bed 'choking' condition [32, 39] in order to maximize the circulation capacity of the inlet jet. The cathode-anode separation distance should be set as close as possible without causing the moving bed of particles to jam or short-circuit to the anode.

The electrochemical kinetics of the SBER cathode can be adequately described by the Tafel equations, incorporating a backstripping reaction. Concentration against time behaviour, obtained by integrating a batch-type differential equation model, was shown to agree reasonably well with the experimental data. The model results also seem to confirm the presence of anodic zones, since backstripping rates from two to ten times those measured by simply shutting off the current were necessary in order to fit the experimental results.

In conclusion, the SBER is a highly coupled electrodynamic/hydrodynamic system. Optimization of the performance of such a system for a particular application requires the proper consideration of a number of factors, some of which have that have been set forth here. It is felt that this can best be performed with the aid of an appropriate electrodynamic/hydrodynamic model that is currently under development.

Acknowledgement

This research was supported by a grant from the US Environmental Protection Agency's Science to Achieve Results (STAR) program under Grant R82-6165.

References

1. R.W. Houghton and A.T. Kuhn, *J. Appl. Electrochem.* **4** (1974) 173.
2. S. Germain and F. Goodridge, *Electrochim. Acta* **21** (1976) 545.
3. F. Coeuret, *J. Appl. Electrochem.* **10** (1980) 687.
4. Dz.E. Hadzismajlovic, K.I. Popov and M.G. Pavlovic, *Powder Technol.* **86** (1996) 145.
5. J.M. Bisang, *J. Appl. Electrochem.* **26** (1996) 135.
6. V. Jiricny, A. Roy and J.W. Evans, *Metall. Mat. Trans. B* **33b** (2002) 669.
7. V.D. Stankovic and S. Stankovic, *J. Appl. Electrochem.* **21** (1991) 124.
8. I.F. Masterson and J.W. Evans, *Metall. Mat. Trans. B* **13b** (1982) 3.
9. K. Scott, *J. Appl. Electrochem.* **18** (1988) 504.
10. V. Jiricny, A. Roy and J.W. Evans, *Metall. Mat. Trans. B* **31b** (2000) 755.
11. F. Goodridge, K. Lister and K. Scott, *J. Appl. Electrochem.* **11** (1981) 723.
12. F. Lapicque and A. Storck, *J. Appl. Electrochem.* **15** (1985) 925.
13. E. Wilhelm, R. Battino and R.J. Wilcock, *Chem. Rev.* **77** (1977) 219.
14. D.J.G. Ives and A.E. Rawson, *J. Electrochem. Soc.* **109** (1962) 447.
15. K. Scott, *J. Chem. Tech. Biotech.* **54** (1992) 257.
16. K. Scott, I.F. McConvey and A.N. Hains, *J. Appl. Electrochem.* **17** (1987) 925.
17. A.T.S. Walker and A.A. Wragg, *Electrochim. Acta* **22** (1977) 1129.

18. C.M.A. Brett, and A.M.O. Brett, 'Electrochemistry: Principles, Methods and Applications' (Oxford Press, Oxford, 1993), p. 74.
19. R. Tamamushi, 'Kinetic Parameters of Electrode Reactions of Metallic Compounds' (Butterworths, UK; 1975) p. vi.
20. R. Tamamushi, *op. cit*. [19], p. 53.
21. B.E. Conway, 'Electrochemical Data', (Elsevier, Amsterdam, 1952) p. 344.
22. D.J. Pickett, 'Electrochemical Reactor Design', (Elsevier, Amsterdam, 2nd edn, 1979), p. 161.
23. E. Kreyszig, 'Advanced Engineering Mathematics' (Wiley, New York, 1999), p. 848.
24. E. Kreyszig, *op. cit*. [23], p. 948.
25. T. Huh and J.W. Evans, *J. Eletrochem. Soc.* **134** (1987) 308.
26. J.O'M. Bockris and A.K.N. Reddy, 'Modern Electrochemistry', Vol. 2 (Plenum Press, New York, 1970) p. 722.
27. D. Hutin and F. Coeuret, *J. Appl. Electrochem.* **7** (1977) 463.
28. J.Y. Bareau and F. Coeuret, *J. Appl. Electrochem.* **9** (1979) 737.
29. A. Storck, M.A. Enriquez-Grandos, M. Roger and F. Coeuret, *Electrochim. Acta* **27** (1982) 293.
30. M.A. Enriquez-Grandos, D. Hutin and A. Storck, *Electrochim. Acta* **27** (1982) 303.
31. K. Kusakabe and S. Morooka, *J. Chem. Eng. Japan* **15** (1981) 208.
32. P.A., Shirvanian, J.M. Calo and G. Hradil, FE-10B, 2001 ASME International Mechanical Engineering Congress and Exposition, New York; accepted for publication in *Int. J. Multiphase Flow* (2004).
33. F. Goodridge, *Electrochim. Acta* **22** (1977) 929.
34. M.M. Saleh, J.W. Weidner, B.E. El-Anadouli and B.G. Ateya, *J. Electrochem. Soc.* **142** (1995) 4122.
35. T. Doherty, J.G. Sunderland, E.P.L. Roberts and D.J. Pickett, *Electrochim. Acta* **41** (1996) 519.
36. B.J. Sabacky and J.W. Evans, *J. Electrochem. Soc.* **126** (1979) 1176.
37. K. Scott, *Electrochim. Acta* **29** (1983) 1191.
38. P.A. Shirvanian, J.M. Calo and G. Hradil, Paper 138c, AIChE Annual Meeting, Indianapolis, IN (2002).
39. J.M. Calo, P.A. Shirvanian, G. Hradil and M. Wyspianski, Symposium Paper 50, Division of Environmental Chemistry, American Chemical Society National Meeting, Boston, MA (2002).